RSC Advances

PAPER

View Article Online
View Journal | View Issue

Cite this: *RSC Adv.*, 2018, **8**, 6315

One-step preparation of a novel $SrCO_3$/g-C_3N_4 nano-composite and its application in selective adsorption of crystal violet

Peng Lu,[a] Xueli Hu,[b] Yujie Li,[a] Meng Zhang,[a] Xiaoping Liu,[b] Youzhou He,[b] Fan Dong,[b] Min Fu[b] and Zhi Zhang*[a]

A novel kind of nanoparticle $SrCO_3$/g-C_3N_4 was prepared using strontium carbonate ($SrCO_3$) and melamine ($C_3H_6N_6$) as raw materials *via* one-step calcination. The formation of $SrCO_3$/g-C_3N_4 was confirmed from the X-ray diffraction (XRD), Fourier transform infrared spectra (FT-IR), Scanning Electron Microscopy (SEM), Transmission Electron Microscopy (TEM), Brunauer–Emmett–Teller (BET) and X-ray photoelectron spectroscopy (XPS) analysis. Its selective adsorption performance was evaluated towards crystal violet (CV), rhodamine B (RhB) and methylene blue (MB). The results showed that the $SrCO_3$/g-C_3N_4 had selective adsorption ability of CV. Furthermore, adsorption measurements of CV were conducted to investigate the influences of contact time, initial concentration, initial dye solution pH value and adsorbent dosage. The maximum removal rate of CV was 98.56% when the initial concentration was 1600 mg L^{-1}. The kinetic study indicated the adsorption of CV followed the pseudo-second-second model well. The adsorption efficiency of $SrCO_3$/g-C_3N_4 was greater (97.46%) than that of g-C_3N_4 (31.30%) and $SrCO_3$ (17.30%). It could be deduced that the synergistic effect of conjugation interaction of g-C_3N_4 and the electrostatic attraction of $SrCO_3$ might be the main driving force for the superb adsorption of CV.

Received 19th October 2017
Accepted 31st January 2018

DOI: 10.1039/c7ra11565b

rsc.li/rsc-advances

1 Introduction

Nowadays, graphitic carbon nitride (g-C_3N_4) has gained considerable research attention because it possesses excellent advantages such as high chemical and thermal stability under ambient temperature, cost-effective, non-toxic and simple preparation.[1,2] g-C_3N_4, as a new intriguing class of graphite analogue, consists of conjugated planes containing highly ordered tri-*s*-triazine (C_6N_7) units. The layered structure of the tri-*s*-triazine is connected by weak forces-van der Waal forces. It has been widely used in the photocatalysis field for it has an energy band gap of 2.7 eV which makes it is capable of the visible adsorption.[3–6] As a photocatalyst, it has been widely used in water splitting,[7,8] organic pollutants degradation,[9,10] CO_2 reduction,[11] and other fields.[12,13]

Crystal violet (CV, $C_{25}H_{30}ClN_3$, IUPAC name is *N*-[4-[bis][4-dimethyl-amino]-phenyl]methylene]-2,5-cyclohexadien-1-yli-dine]-*n*-methylmethanaminium chloride), a typical triphenyl-methane dye, is widely used in cell biology, paper, leather and textile industry.[14–16] The wastewater containing CV is low biodegradability and high stability (complex aromatic structure) and it could be absorbed through the skin and causing the skin, eye, digestive irritation and even cancer.[17–19] From the aspect of environmental safety and health of life, it is vital to develop an effective way to abate CV in wastewater. Various methods have been adopted for eliminating dye pollution from water, including chemical oxidation,[20,21] photo-catalytic decomposition,[22,23] electro-catalytic degradation[24,25] and non-thermal plasma.[26–28] These methods usually have some defects, such as slow degradation rate, complex, heavy expenses and usually causing secondary pollution. The adsorption technique is gaining more attention for it is high efficiency, simple design, cost-effective and adaptable.[29–35] There have been various kinds of adsorbents developed, such as carbon materials,[36–38] natural clay minerals,[39–42] and bioadsorbents.[43–45] However, certain deficiencies including costly, intricate pre-treatment and low adsorption capability limited the use of some certain adsorbents.[46–53]

Due to the conjugated region, stacking structure and the weak forces of g-C_3N_4, it has the potential for aggregating functional groups or materials to form nanocomposite with multiform favorable properties.[54–56] This distinctive structure has drawn great interesting in improving the photocatalytic performance.[57,58] But the research of using modified g-C_3N_4 as adsorbent for clearing up dye pollutant is rarely been reported.[59,60] As far as we know, there has been no report of using

[a]*College of Urban Construction and Environmental Engineering, Chongqing University, Chongqing 400045, China. E-mail: zhangzhicqu2016@126.com*

[b]*College of Environment and Resources, Chongqing Technology and Business University, Chongqing Key Laboratory of Catalysis and New Environmental Materials, Chongqing 400067, China*

g-C_3N_4-based composite as an adsorbent in dye wastewater treatment. Strontium carbonate ($SrCO_3$), a typical alkaline earth metal carbonate, has been widely used as additives in industrial production.[61–63] Meanwhile, some research has been reported on its adsorption performance attributed to its various architectures.[64,65]

In this work, we firstly induced $SrCO_3$ to incorporate with g-C_3N_4 *via* one-step calcination method to fabricate a novel adsorbent $SrCO_3$/g-C_3N_4. The morphology and structure of the composite was characterized by XRD, FT-IR, SEM, TEM, BET and XPS, and its adsorptive capacity and selectivity of CV in aqueous solution were investigated. To the best of our knowledge, this work represents the first example employing g-C_3N_4-based composite for selective adsorption of CV.

2 Experimental

2.1 Synthesis of $SrCO_3$/g-C_3N_4

$SrCO_3$, melamine and CV are all AR grade and purchased from Chengdu Kelong Chemical Agents (China), without any further purification. $SrCO_3$/g-C_3N_4 was synthesized by one-step calcination process in a muffle furnace. $SrCO_3$ and melamine (mass ratio = 1 : 1) were dissolved with deionized water in alumina crucible, and then the mixed solution was dispersion with ultrasonic irradiation for 20 min under ambient temperature. The final solution was transferred into muffle furnace and maintained at 600 °C for 4 hours at heating rate of 5 °C min^{-1} to obtain the prepared nanocomposite. $SrCO_3$ and melamine were also treated as the forward route for making comparison.

2.2 Characterization

X-ray diffraction (XRD, Shimadzu, XRD-6100) patterns were detected with Cu Kα radiation (40 kV, 30 mA, 2θ = 10–80°) to investigate the crystal structures of the samples. Fourier transform infrared spectra (FT-IR, Shimadzu, IR Prestige-21), were recorded in the range of 4500–400 cm^{-1}, using KBr technique to analyze the functional groups on the surface of the composite. Scanning electron microscope (SEM, JEOL, JSM-7800F) and Transmission Electron Microscopy (TEM, JEOL, JEM-2100) were used to observe the morphologies and the microstructures of the samples. The N_2 adsorption apparatus (Micromeritics, ASAP 2020) were used to obtain the Brunauer–Emmett–Teller (BET) surface area of the samples. X-ray photoelectron spectroscopy (XPS, Thermo Scientific, ESCALAB 250xi) was used to determine the binding energy.

2.3 Adsorption experiments

The concentration of CV in the solution was determined at the maximum absorbance (λ_{max} = 580 nm) by UV-vis spectrophotometer (UV-vis spectrometer, Tianmei, UV1102). For high concentration, the samples were diluted before measurements. And the initial pH of the dye solution was measured by pH meter (pH meter, Sartorius, PB10).

The adsorption experiments were conducted by a batch method. All experiments were conducted at 7.0 pH value, except those that investigated the effect of initial pH of dye solution. And 0.08 g adsorbent was dispersed in 80 mL CV solution, except that were used to study the effect of the dosage. Similarly, the initial concentration is 1600 mg L^{-1}, except those that investigate the same parameters. The pH of the initial dye solution was adjusted with HCL (0.1 mol L^{-1}) and NaOH (0.1 mol L^{-1}). The kinetic experiments were carried out at the initial concentration of 500, 1000, 1200, 1400, and 1600 mg L^{-1}. It performed on an air bathed shaker. The solution was separated by centrifugation at 5000 rpm for 5 min.

The adsorption capacity at time t q_t (mg g^{-1}) and removal rate (%) were calculated using the following equation:

$$q_t = \frac{(C_0 - C_t) \times V}{m} \quad (1)$$

$$\text{Removal rate } (\%) = \frac{C_0 - C_t}{C_0} \times 100 \quad (2)$$

where C_0 and C_t are the liquid-phase concentrations of the CV (mg L^{-1}) at initial time and time t, respectively. V is the volume of the solution (mL) and m is the mass of the used adsorbent (mg).

3 Results and discussion

3.1 Characterization of the samples

The XRD patterns of the prepared samples are shown in Fig. 1. The g-C_3N_4 displayed a typical diffraction peaks at 27.46° and 12.96°, corresponding to the (002) and (100) diffraction planes, which represented the interlayer stacking reflection and in-plane structure of aromatic system, respectively.[66,67] This indicated that the g-C_3N_4 was synthesized by polycondensation approach with pure melamine. Meanwhile, the observed diffraction peaks of calcined $SrCO_3$ are located at 2θ angles = 25.28°, 25.91°, 29.73°, 31.62°, 34.64°, 35.22°, 36.64°, 41.42°, 44.18°, 45.74°, 46.68°, 47.80°, 50.03° which correspond to the planes of (111), (021), (002), (012), (102), (200), (130), (220), (221), (041), (202), (132), (113), respectively. It could be unambiguously indexed to the orthorhombic phase of $SrCO_3$ (JCPDS card no. 05-0418).[68,69] There is no observation of the typical

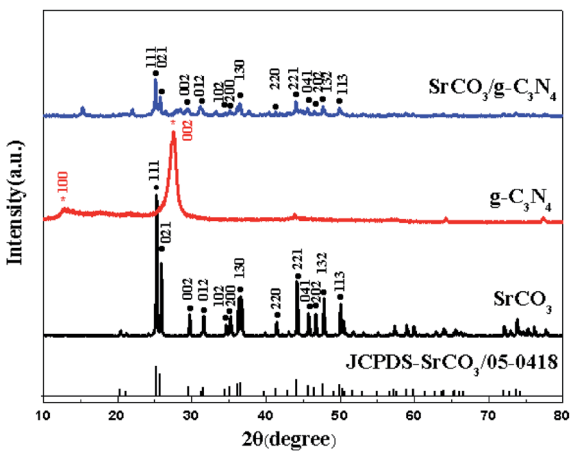

Fig. 1 XRD patterns of the g-C_3N_4, $SrCO_3$ and $SrCO_3$/g-C_3N_4.

diffraction of g-C_3N_4 in the synthesized composite, the diffraction peaks were mostly the same as the $SrCO_3$, but the feature peaks positions of $SrCO_3$ shifted slightly toward a lower diffraction angle. And the impure peaks of the composite might be the carbonization of the raw materials or the melamine did not condense completely.

The FT-IR spectra of the prepared materials are shown in Fig. 2. For the calcined melamine, the typical adsorption peaks in the 1200–1700 cm^{-1} range and at 808 cm^{-1} of g-C_3N_4 could be observed. They are assigned to the typical skeletal stretching vibrations of armomatic C–N heterocycles and the out-of-plane bending vibration of tri-*s*-triazine rings, respectively.[70,71] The peaks at 698, 858, 1070, 1458 and 1774 cm^{-1} corresponding to the CO_3^{2-} of the calcined $SrCO_3$ were observed.[50] In case of the $SrCO_3$/g-C_3N_4, the typical skeletal stretching vibrations of tri-*s*-triazine were hardly observed; it might be the adsorption intense of $SrCO_3$ was so strong in order to impede the peaks of g-C_3N_4. Meanwhile, the peak at 808 cm^{-1} presented in g-C_3N_4 shifted to 821 cm^{-1}, the peak at 856 cm^{-1} presented in $SrCO_3$ shifted to 858 cm^{-1}, the peaks at 1070 cm^{-1} and 1774 cm^{-1} were disappeared, these might due to the strong interactions between the carbonate of $SrCO_3$ and tri-*s*-triazine rings of g-C_3N_4. Furthermore, the new peak at 2112 cm^{-1} corresponding to C≡N groups appeared after calcination indicating that the incorporation of $SrCO_3$ has intense interaction during the condense process of melamine.[72]

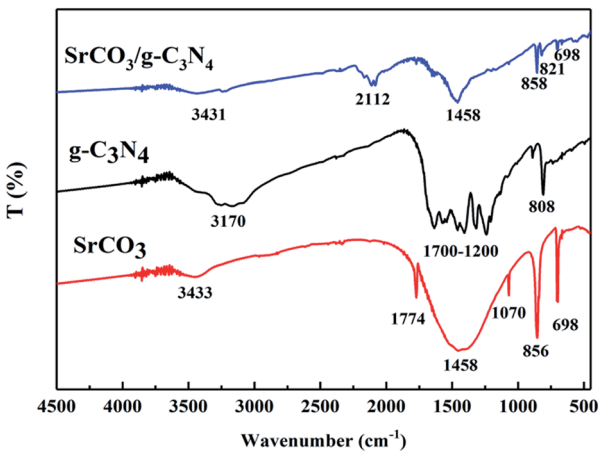

Fig. 2 FT-IR spectra of the g-C_3N_4, $SrCO_3$ and $SrCO_3$/g-C_3N_4.

To make further investigation of the constitution of the prepared composite, the calcined product was treated with HCl (0.5 mol L^{-1}) and deionized water, because g-C_3N_4 possessed fascinating acid stability. The treatment was terminated until the pH value was neutral, and then the treated nanocomposite was dried at 60 °C for 24 h. The XRD patterns and FT-IR spectra of the HCl-treated product are characterized in Fig. 3. The feature diffraction peak of g-C_3N_4, indicating the interlayer stacking, changed from 27.46° to 27.92° is explicitly observed in Fig. 3a. The change of the diffraction peak was corresponded to the stacking distance reduced from 0.325 to 0.319 nm. The above results implied that the interlayer stacking order was improved. And FT-IR spectra of the product were well matched with the pure g-C_3N_4 except the weak intensity (Fig. 3b). So, it could be indicated that the $SrCO_3$/g-C_3N_4 was formed with the raw materials $SrCO_3$ and melamine.

SEM and TEM images of the calcined samples are displayed in Fig. 4. It revealed the morphology and microstructure of $SrCO_3$/g-C_3N_4. In Fig. 4a, it could be seen the calcined melamine was predominantly composed of plate-like sheets,[73] and the morphology of calcined $SrCO_3$ was irregular polyhedrons with smooth surface is shown in Fig. 4b. In Fig. 4c, it could be seen clearly that the g-C_3N_4 covered on the $SrCO_3$ incompletely. Further structural details of $SrCO_3$/g-C_3N_4 are shown in Fig. 4d. There were some step edges of the layered g-C_3N_4 and rods-like $SrCO_3$ with some parts overlapping. It might be the amount of g-C_3N_4 was not enough to disperse on the entire surface of $SrCO_3$; and some areas cannot be wrapped by the g-C_3N_4. The SEM and TEM image could reveal that there existed some interactions between these two materials. Meanwhile, the specific surface areas of the clained samples were measured. As shown in Table 1, compared with g-C_3N_4 the composite BET surface area gets smaller with the addition of $SrCO_3$, this might be the $SrCO_3$ interacted with the stacking structure of g-C_3N_4. These results

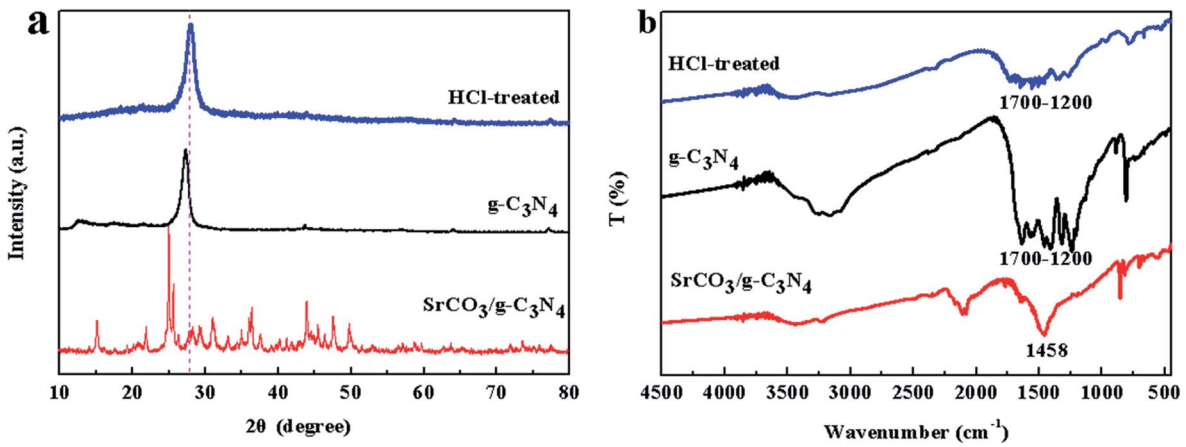

Fig. 3 XRD patterns (a) and FT-IR spectra (b) of the HCl-treated $SrCO_3$/g-C_3N_4.

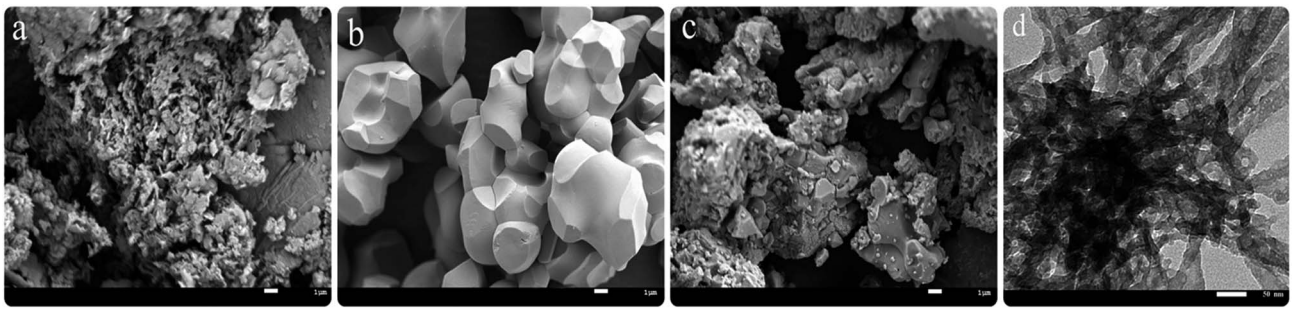

Fig. 4 SEM images of the g-C_3N_4 (a), $SrCO_3$ (b) and $SrCO_3$/g-C_3N_4 (c); TEM images of the $SrCO_3$/g-C_3N_4 (d).

Table 1 Textural properties of g-C_3N_4, $SrCO_3$ and $SrCO_3$/g-C_3N_4[a]

Sample	S_{BET} (m^2 g^{-1})	V_{total} (cm^3 g^{-1})	D (nm)
g-C_3N_4	27.4	0.126	17.5
$SrCO_3$	1.93	0.003	8.72
$SrCO_3$/g-C_3N_4	5.86	0.016	9.69

[a] S_{BET}: BET surface area, V_{total}: total pore volume, D: average pore diameter calculated using BJH method.

consistent with SEM results which could further prove that there have been some interactions between $SrCO_3$ and g-C_3N_4.

To further study the chemical state of $SrCO_3$/g-C_3N_4, the XPS measurements were carried out. Fig. 5a is the general XPS spectra of calcined materials, indicating the presence of C, N, O and Sr in $SrCO_3$/g-C_3N_4. The XPS spectra of C 1s are shown in Fig. 5b. For pristine g-C_3N_4 the peaks at 284.2 eV, 287.7 eV were corresponding to sp^2-hybridized carbon in C–C group or the adventitious hydrocarbon[74] and sp^2-bond carbon in form of C–C=N.[75] But after the blended calcinations, the peak at 284.2 eV shifted to 284.6 eV. The N 1s spectra are shown in Fig. 5c. The peak at 398.2 eV was attributed to sp^2-hybridized nitrogen in N atom aromatic rings in form of C–N=C,[76] and the nearly peaks at 399.3 eV and 401.0 eV were regarded as tertiary nitrogen (N-$(C)_3$) and amino functional groups, respectively.[77] After incorporation, the binding energy peaks slightly shifted. The peaks at 531.1 eV and 533.2 eV of O 1s spectra corresponding to the $SrCO_3$ have no significant change in Fig. 5d. The XPS spectra of Sr 3d at 133.1 eV and 134.6 eV for calcined $SrCO_3$ were observed in Fig. 5e. These peaks was corresponding to the Sr 3d5/2 and Sr 3d3/2, and the peak at 134.6 eV shifted to 134.7 eV after calcination. All these changes after co-calcination suggested that there were strong interactions between the two raw materials. Therefore, according to the analysis of XPS and the above results of XRD, FT-IR, SEM, TEM and BET measurements, it could be concluded that the $SrCO_3$/g-C_3N_4 was synthesized using $SrCO_3$ and melamine by one-step calcination.

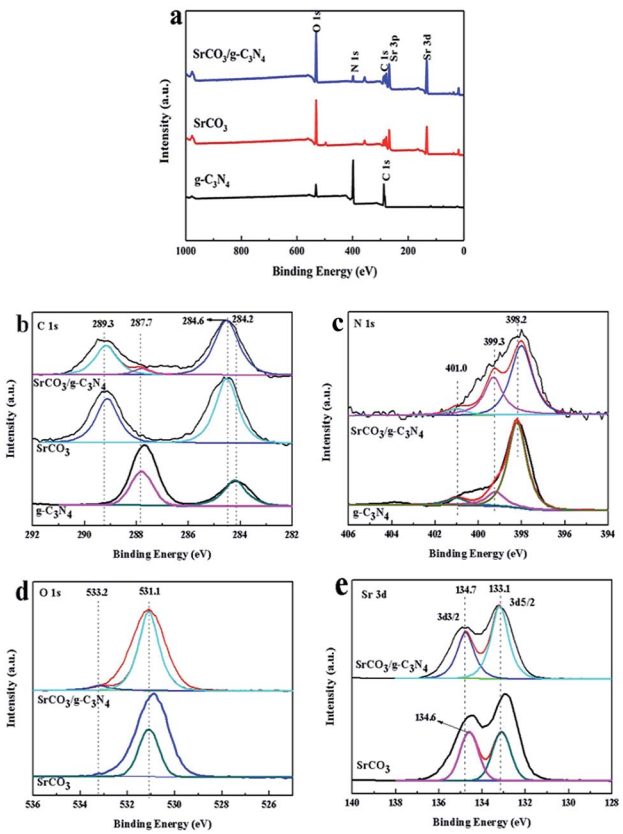

Fig. 5 XPS survey spectra of g-C_3N_4, $SrCO_3$ and $SrCO_3$/g-C_3N_4 (a) and high-resolution XPS spectrum: C 1s (b), N 1s (c), O 1s (d) and Sr 3d (e).

3.2 The selective adsorption of CV

In our previous study, cationic dyes MB, RhB and CV were chosen as the target dye to conduct the adsorption experiments. We found that $SrCO_3$/g-C_3N_4 appeared efficient adsorption capacity for CV except for the other dye solutions. To make further investigation of the selectivity of $SrCO_3$/g-C_3N_4, mixed solutions of CV/MB, CV/RhB and CV/MB/RhB with equal volume ratio were prepared. The concentration of each dye solution was 10 mg L^{-1}, and dosage ratio of $SrCO_3$/g-C_3N_4 and mixed solutions was 1 g L^{-1}. The adsorption experiments were carried out under ambient temperature and different pH value for 120 min.

The optical pictures and UV-vis measurements of the adsorption process are shown in Fig. 6. It could be apparently seen that CV was decolorized after the test (Fig. 6b), but in the MB and RhB groups the color slightly changed (Fig. 6a–c). In Fig. 6d, the color of CV/MB mixed solution was changed from dark blue to incipient blue (the color corresponding to the MB). For the CV/RhB group, the end color is very close to RhB

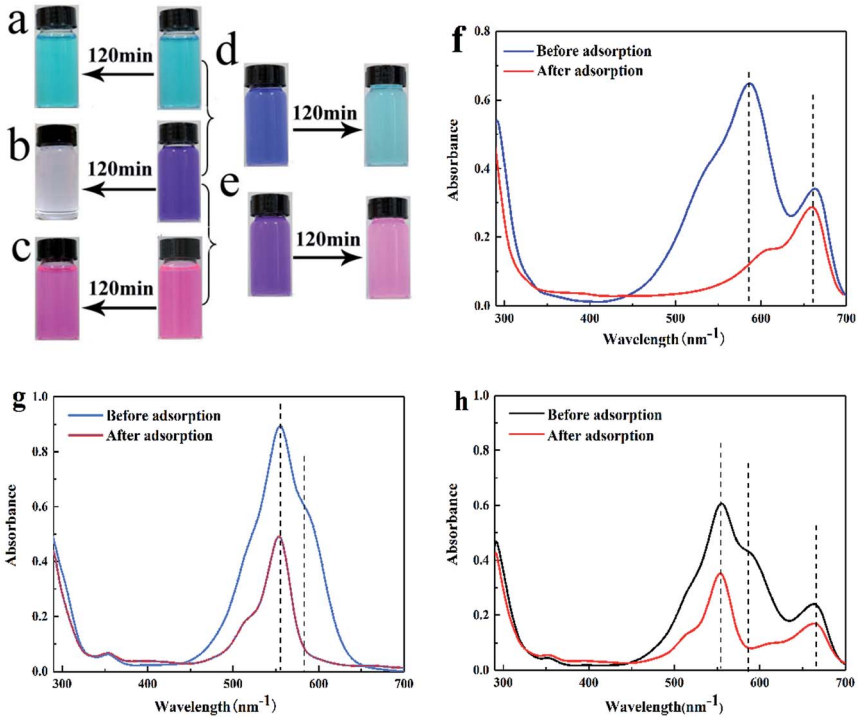

Fig. 6 Optical photographs of single adsorption of MB (a), CV (b) and RhB (c); the selective adsorption of CV from CV/MB (d) and CV/RhB (e) mixture, UV-vis spectra of CV/MB (f),CV/RhB (g) and CV/MB/RhB (h) mixture before and after adsorption.

(Fig. 6e). It suggested that CV in these two mixtures was selectively captured. However, the color in group CV/MB/RhB did not change, because the color of MB and RhB mixed solution is the same as that of CV. To further investigate the selective adsorption of CV, the UV-vis spectra were conducted for the tested groups. In the case of CV/MB, the UV-vis adsorption peaks of CV and MB were at 580 nm and 664 nm before adsorption, respectively. After adsorption, the peak of CV was dropped down drastically while the MB peak was almost unchanged (Fig. 6f). The same situation happened in the CV/RhB group (Fig. 6g). Although the optical of CV/MB/RhB group did not change, but the UV-vis adsorption curve appeared the same situation with the other two mixed groups (Fig. 6h). It could be concluded that the $SrCO_3$/g-C_3N_4 performed selective adsorption of CV from CV/MB/RhB.

Furthermore, we also evaluated the effect of the initial pH of the dye solution. Fig. 7 shows the tested results. It could be seen that the initial pH (ranged from 4 to 10) of mixed dye solution did not significantly influence the adsorption process in each tested group.

3.2.1 Effect of contact time. Fig. 8 shows the effect of different contact time (0–160 min) in the adsorption process. The initial concentration of CV is 1600, 1800 and 2000 mg L^{-1} and the dosage ratio of $SrCO_3$/g-C_3N_4 and CV solution was 1 g L^{-1}. For all concentrations, the removal rate of CV became constant after 120 min. Meanwhile, the group of 1600 mg L^{-1} reached the equilibrium firstly and the removal rate was up to the other concentration. So, the contact time of 120 min and the initial concentration of CV of 1600 mg L^{-1} were chosen for the following investigation.

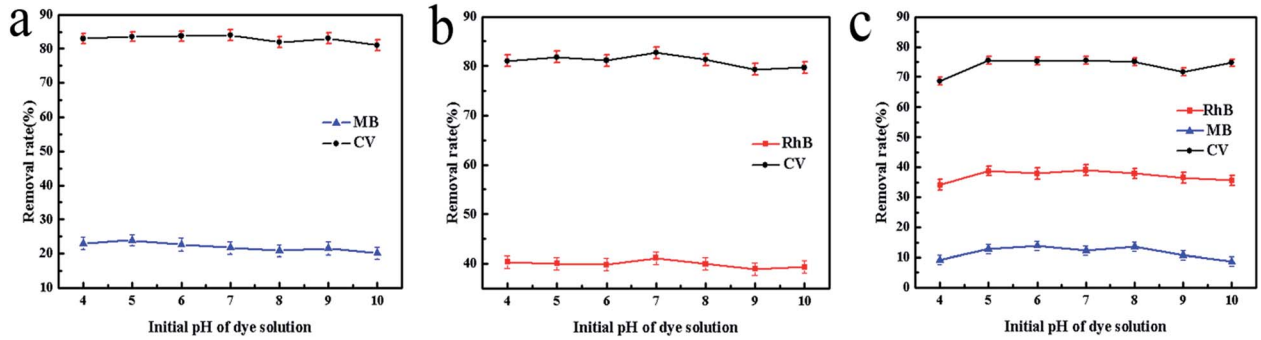

Fig. 7 Effect of the initial pH of mixed dye solution CV/MB (a), CV/RhB (b) and CV/MB/RhB (c).

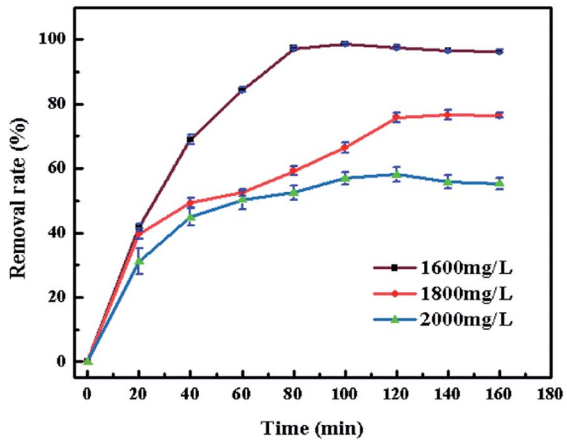

Fig. 8 Effect of contact time.

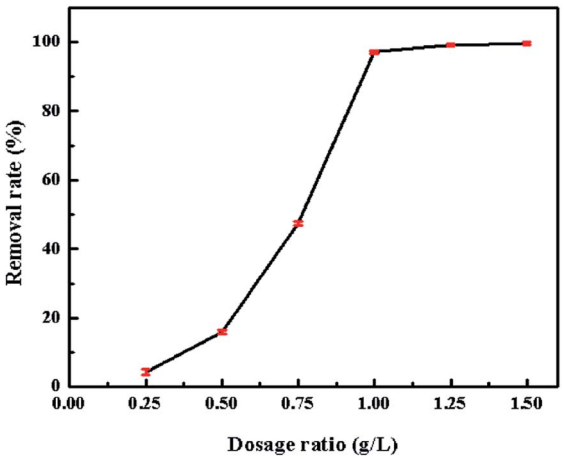

Fig. 10 Effect of $SrCO_3$/g-C_3N_4 dosage.

3.2.2 Effect of initial concentration of CV. The effect of initial concentration (50–2000 mg L^{-1}) of CV is shown in Fig. 9. From the obtained results, it was found that the removal efficiency kept steadily before the initial dye concentration up to 1800 mg L^{-1}. This might be attributed to the higher initial concentration offered more numbers of dye molecules that could contact easily with $SrCO_3$/g-C_3N_4. However, the removal rate was reduced at higher initial concentration indicating the saturation of $SrCO_3$/g-C_3N_4.

3.2.3 Effect of adsorbent dosage. The dosage of the adsorbents is one of the major parameter which influences the adsorption process; an appropriate amount of adsorbents is in favor of the real industrial treatment. Fig. 10 shows the effect of the adsorbent dosage (0.25, 0.50, 0.75, 1.00, 1.25, 1.50 g L^{-1}) of the CV. The removal rate increased with the increased amount of the adsorbent. When the dosage ups to 1.00 g L^{-1}, the removal efficiency did not increase with the increasing dosage. It might due to the binding of almost CV ions onto $SrCO_3$/g-C_3N_4, which made the equilibrium between solution and adsorbents. So the amount of adsorbent 1.00 g L^{-1} was the suitable dosage for the adsorption of CV.

3.2.4 Effect of pH. The pH of initial dye solution is a key factor in adsorption process, which could influence the interaction between adsorbent and dye. In order to find out the pH effect, the adsorption test was conducted at initial solution pH ranged from 4 to 10. The results in Fig. 11 show that the initial pH of CV solution had little effect on the adsorption capacity. This observation could demonstrate that $SrCO_3$/g-C_3N_4 is suitable for removing CV in wastewater in a wide pH range, and there is no need to adjust the initial solution pH before treatment.

3.3 Adsorption kinetics

In order to study the characteristics of the adsorption process, pseudo-first-order and pseudo-second-order kinetics models were carried out with different concentration (500, 1000, 1200, 1600 mg L^{-1}). The pseudo-first-order and pseudo-second-order are expressed by eqn (3) and (4).[78]

$$\ln(q_e - q_t) = \ln q_e - k_1 t \quad (3)$$

$$\frac{t}{q_t} = \frac{1}{k_2 q_e^2} + \frac{t}{q_e} \quad (4)$$

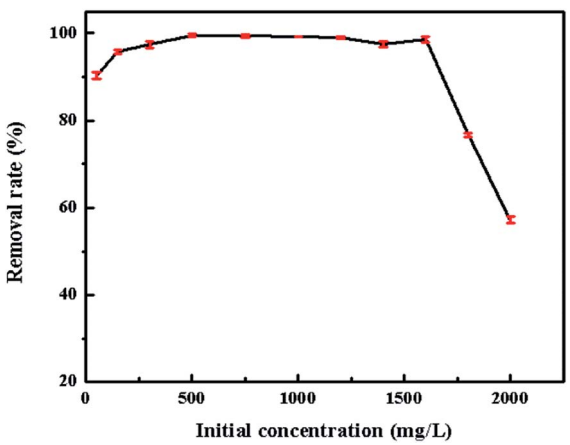

Fig. 9 Effect of initial CV concentration.

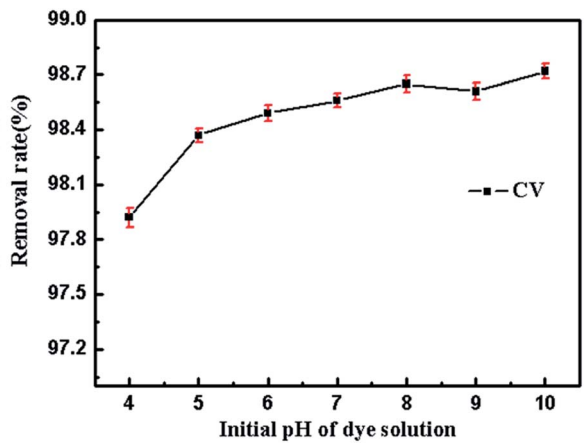

Fig. 11 Effect of the initial pH of CV.

where k_1 (min^{-1}) and k_2 (g (mg^{-1} min^{-1})) are the rate constant of pseudo-first-order and pseudo-second-order model, respectively; q_e (mg g^{-1}) and q_t (mg g^{-1}) are the adsorbed amount at equilibrium time and time t.

The rate constant of adsorption could be calculated from the slope of the plot in Fig. 12 and was listed in Table 2. R^2 of pseudo-second-order model is much higher than the other, indicating that the pseudo-second order equation is more suitable to describe the CV adsorption with $SrCO_3$/g-C_3N_4. So the chemisorptions or chemical sorption was the rate-controlling step for the adsorption process.[79]

3.4 Desorption and reuse

In order to evaluate the reusability of $SrCO_3$/g-C_3N_4, the regeneration process was performed. Adsorption experiment was conducted at the optimal condition as ascribed above in a 250 mL CV solution firstly, after equilibrium the used adsorbent was regenerated by centrifugation and washed several times with methanol and water at room temperature. Finally, the regenerated composite was dried for 24 h at 60 °C for reusing.

It could be seen that the removal rate gradually decreased after regeneration in Fig. 13. It might conclude that the adsorption mechanism of this process is not due to the physical adsorption.

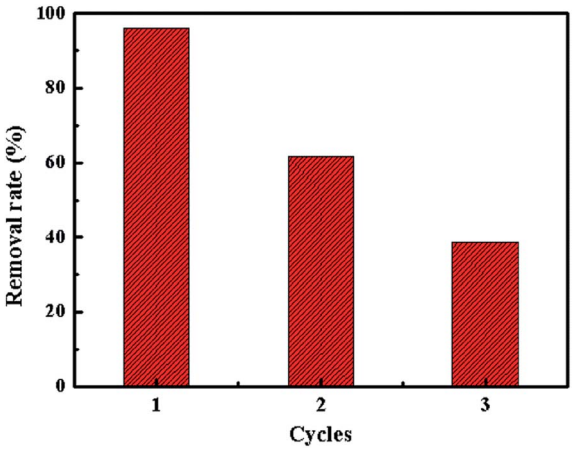

Fig. 13 Reusability of the adsorbent.

3.5 Adsorption mechanism of crystal violet

To further study the adsorption performance of CV, the adsorption experiments were conducted with the calcined $SrCO_3$, g-C_3N_4 and $SrCO_3$/g-C_3N_4 firstly. 0.08 g tested materials were dispersed in 80 mL CV solution (10 mg L^{-1}), respectively. After 2 h adsorption process, the removal rate of CV for tested materials is exhibited in Fig. 14. It could be seen obviously that the removal ability of g-C_3N_4 and $SrCO_3$ to CV is much smaller than that of the nanocomposite. The removal rate of g-C_3N_4, $SrCO_3$ and $SrCO_3$/g-C_3N_4 were 31.30%, 17.30% and 97.46%, respectively. The adsorption mechanism of g-C_3N_4 might be attributed to π–π interaction between the g-C_3N_4 and CV, and that for the $SrCO_3$, the electrostatic attraction between the carbonate generated from the hydrolytic of $SrCO_3$ and the cationic chromogenic groups of CV. And for the $SrCO_3$/g-C_3N_4, the synergistic effect of π–π interaction and electrostatic attraction highly improved the adsorption properties of the

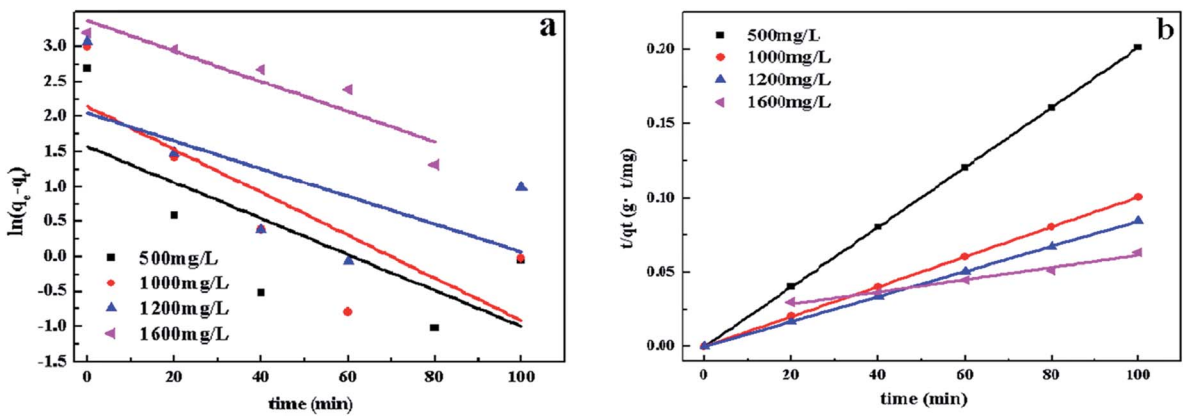

Fig. 12 Pseudo-first-order (a), and pseudo-second-order (b) kinetic plots for adsorption.

Table 2 Kinetic parameters of different initial CV concentration

	Pseudo-first-order			Pseudo-second-order			
C_0 (mg L^{-1})	q_e (cal) (mg g^{-1})	k_1 (min^{-1})	R^2	q_e (exp) (mg g^{-1})	q_e (cal) (mg g^{-1})	k_2 (g (mg^{-1} min^{-1})) × 10^{-5}	R^2
1600	16.91	0.014	0.5357	1576.9	1666.7	3.67	0.9425
1800	28.33	0.016	0.7481	1378.6	1428.5	3.53	0.9577
2000	29.53	0.024	0.7822	1143.4	1250.0	8.10	0.9902

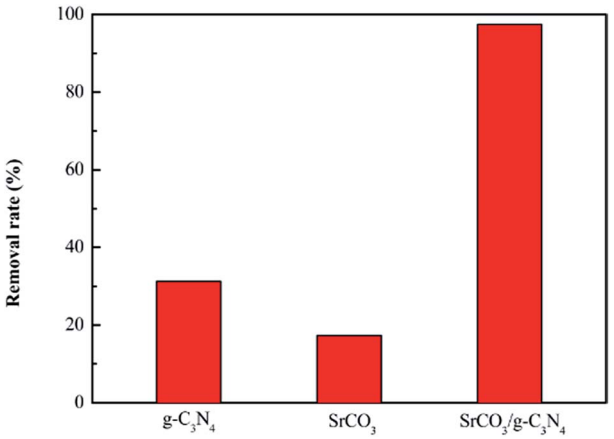

Fig. 14 Comparisons of the adsorption effect of the $SrCO_3$, g-C_3N_4, and $SrCO_3$/g-C_3N_4.

nanocomposite on CV.[50] According to the above results and the crystal structures, we could deduce that superb adsorption capacity of CV might attribute to the synergistic interaction of the conjugation of g-C_3N_4 and the electrostatic attraction of $SrCO_3$.

Furthermore, the FT-IR spectra of $SrCO_3$/g-C_3N_4 before and after CV adsorption were recorded. As shown in Fig. 15, the peak at 2112 cm^{-1} assigned to the nitrile groups shifted to the 2107 cm^{-1} and the peak at 1319 cm^{-1} assigned to aromatic C–N heterocycles observed clearly. These results indicate that the previously mentioned groups are involved in the adsorption process. Moreover, the intensity of the peak 1458 cm^{-1} corresponding to C–N heterocycle aromatic became stronger, that was for the CV was adsorbed onto the $SrCO_3$/g-C_3N_4. All the changes of the FT-IR spectra of the $SrCO_3$/g-C_3N_4 before and after adsorption could indicate that there have been intense interactions between dye molecules and $SrCO_3$/g-C_3N_4. Furthermore, the result of desorption test might indicate that there has been intense chemical adsorption between the composite and CV. It could deduced that $SrCO_3$/g-C_3N_4 performed selective adsorption of CV might due to the chemical

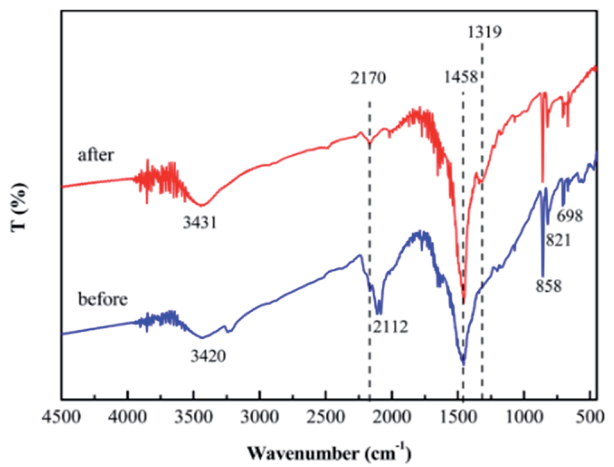

Fig. 15 FT-IR spectra of $SrCO_3$/g-C_3N_4 before and after adsorption.

structure of CV is more symmetrical and conjugation degree is higher than MB and RhB. On the basis of the above analysis, the conjugation and electrostatic interaction would be the driving force for the selective adsorption of CV.

4 Conclusions

In summary, a new $SrCO_3$/g-C_3N_4 composite adsorbent was firstly synthesized with $SrCO_3$ and melamine *via* a simple one-step calcination method. The $SrCO_3$/g-C_3N_4 performed high and specific selective adsorption for CV. The experiment data was well described by the pseudo-second-order model. According to the crystal structural feature of $SrCO_3$/g-C_3N_4 and the FT-IR analysis of $SrCO_3$/g-C_3N_4 before and after adsorption of CV, it could be deduced that the synergies of π conjugation and electrostatic interaction would be the mechanism for the selective adsorption of CV. Our findings indicate that g-C_3N_4 based composite $SrCO_3$/g-C_3N_4 could be a promising adsorbent which can potentially be applied for the removal of CV pollutants from aqueous solution.

Conflicts of interest

There are no conflicts to declare.

Acknowledgements

The authors are grateful for the financial support from the National Natural Science Foundation of China (No. 51778082, No. 21502012), Scientific and Technological Research Program of Chongqing Municipal Education Commission (No. KJ1500615, No. KJ130704), Chongqing University Postgraduates Innovation Project (No. CYB15039) and the Natural Science Foundation of Chongqing (No. cstc-2017shmsA20019, No. cstc2017jcyjAX0404).

Notes and references

1 Z. W. Zhao, Y. J. Sun and F. Dong, Graphitic carbon nitride based nanocomposites: a review, *Nanoscale*, 2015, **7**, 15–37.
2 F. Ding, D. Yang, Z. W. Tong, Y. H. Nan, Y. J. Wang, X. Y. Zou and Z. Y. Jiang, Graphitic carbon nitride-based nanocomposites as visible-light driven photocatalysts for environmental purification, *Environ. Sci.: Nano*, 2017, **4**, 1455–1469.
3 X. C. Wang, K. Maeda, A. Thomas, K. Takanabe, G. Xin, J. M. Carlsson, K. Domen and M. Antonietti, A metal-free polymeric photocatalyst for hydrogen production from water under visible light, *Nat. Mater.*, 2009, **8**, 76–80.
4 A. Y. Shi, H. H. Li, S. Yin, B. Liu, J. C. Zhang and Y. H. Wang, Effect of conjugation degree and delocalized π-system on the photocatalytic activity of single layer g-C_3N_4, *Appl. Catal., B*, 2017, **218**, 137–146.
5 M. Wu, J. M. Yan, X. W. Zhang and M. Zhao, Synthesis of g-C_3N_4 with heating acetic acid treated melamine and its photocatalytic activity for hydrogen evolution, *Appl. Surf. Sci.*, 2015, **354**, 196–200.

6 G. Mamba and A. K. Mishra, Graphitic carbon nitride (g-C_3N_4) nanocomposite: A new and exciting generation of visible light driven photocatalysts for environmental pollution remediation, *Appl. Catal., B*, 2016, **198**, 347–377.
7 Y. Zheng, L. H. Lin, B. Wang and X. C. Wang, Graphitic carbon nitride polymers toward sustainable photoredox catalysis, *Angew. Chem., Int. Ed.*, 2015, **54**, 12868–12884.
8 J. Li, Y. C. Yin, E. Z. Liu, Y. N. Ma, J. Wan, J. Fan and X. Y. Hu, *In situ* growing Bi_2MoO_6 on g-C_3N_4 nanosheets with enhanced photocatalytic hydrogen evolution and disinfection of bacteria under visible light irradiation, *J. Hazard. Mater.*, 2017, **321**, 183–192.
9 K. Katsumata, R. Motoyoshi, N. Matsushita and K. Okada, Preparation of graphitic carbon nitride (g-C_3N_4)/WO_3 composites and enhanced visible-light-driven photodegradation of acetaldehyde gas, *J. Hazard. Mater.*, 2013, **260**, 475–482.
10 J. F. Zhang, Y. F. Hu, X. L. Jiang, S. F. Chen, S. G. Meng and X. L. Fu, Design of a direct Z-scheme photocatalyst: Preparation and characterization of Bi_2O_3/g-C_3N_4 with high visible light activity, *J. Hazard. Mater.*, 2014, **280**, 713–722.
11 D. Masih, Y. Y. Ma and S. Rohani, Graphitic C_3N_4 based noble-metal-free photocatalyst systems: A review, *Appl. Catal., B*, 2017, **206**, 556–588.
12 S. W. Liu, F. Chen, S. T. Li, X. X. Peng and Y. Xiong, Enhanced photocatalytic conversion of greenhouse gas CO_2 into solar fuels over g-C_3N_4 nanotubes with decorated transparent ZIF-8 nanoclusters, *Appl. Catal., B*, 2017, **211**, 1–10.
13 F. Wang, G. Wang, J. C. Zhang, B. Q. Li, J. Zhang, J. Deng, J. W. Chen and R. L. Wang, Novel sulfonated poly (ether ether ketone)/oxidized g-C_3N_4 composite membrane for vanadium redox flow battery applications, *J. Electroanal. Chem.*, 2017, **797**, 107–112.
14 A. Mittal, J. Mittal, A. Malviya, D. Kaur and V. K. Gupta, Adsorption of hazardous dye crystal violet from wastewater by waste materials, *J. Colloid Interface Sci.*, 2010, **343**, 463–473.
15 L. Y. Zhang, H. Y. Zhang, W. Guo and Y. Tian, Removal of malachite green and crystal violet cationic dyes from aqueous solution using activated sintering process red mud, *Appl. Clay Sci.*, 2014, **93–94**, 85–93.
16 Y. Y. Pei, M. Wang, D. Tian, X. F. Xu and L. J. Yuan, Synthesis of core–shell SiO_2@MgO with flower like morphology for removal of crystal violet in water, *J. Colloid Interface Sci.*, 2015, **453**, 194–201.
17 V. Sabna, S. G. Thampi and S. Chandrakaran, Adsorption of crystal violet onto functionalized multi-walled carbon nanotubes: Equilibrium and kinetic studies, *Ecotoxicol. Environ. Saf.*, 2016, **134**, 390–397.
18 S. Charkraborty, S. Chowdhury and P. D. Saha, Adsorption of Crystal Violet from aqueous solution onto NaOH-modified rice husk, *Carbohydr. Polym.*, 2011, **86**, 1533–1541.
19 R. Kumar and R. Ahmad, Biosorption of hazardous crystal violet dye from aqueous solution onto treated ginger waste (TGW), *Desalination*, 2011, **265**, 112–118.
20 K. N. Vinod, Puttaswamy and K. N. Ninge Gowda, Oxidative decolorization of triphenylmethane dyes by chloramine-T in alkaline medium catalyzed by Pd(II): A comparative spectrophotometric kinetic and mechanistic approach, *J. Mol. Catal. A: Chem.*, 2009, **298**, 60–68.
21 J. Y. Yin, J. J. Cai, C. Yin, L. F. Gao and J. C. Zhou, Degradation performance of crystal violet over CuO@AC and CeO_2–CuO@AC catalysts using microwave catalytic oxidation degradation method, *J. Environ. Chem. Eng.*, 2016, **4**, 958–964.
22 F. T. Chen, P. F. Fang, Y. P. Gao, Z. Liu, Y. Liu and Y. Q. Dai, Effective removal of high-chroma crystal violet over TiO_2-based nanosheet by adsorption–photocatalytic degradation, *Chem. Eng. J.*, 2012, **204–206**, 107–113.
23 Y. R. Jiang, H. P. Lin, W. H. Chung, Y. M. Dai and C. C. Chen, Controlled hydrothermal synthesis of BiOxCly/BiOmIn composite exhibiting visible-light photocatalytic degradation of crystal violet, *J. Hazard. Mater.*, 2015, **283**, 787–805.
24 S. Popli and U. D. Patel, Mechanistic aspects of electrocatalytic reduction of Reactive Black 5 dye in a divided cell in the presence of silver nano-particles, *Sep. Purif. Technol.*, 2017, **179**, 494–503.
25 X. Y. Zhang, H. Q. Luo and N. B. Li, Crystal violet as an i-motif structure probe for reversible and label-free pH-driven electrochemical switch, *Anal. Biochem.*, 2014, **455**, 55–59.
26 A. Khataee, P. Gholami, B. Vahid and S. W. Joo, Heterogeneous sono-Fenton process using pyrite nanorods prepared by non-thermal plasma for degradation of an anthraquinone dye, *Ultrason. Sonochem.*, 2016, **32**, 357–370.
27 B. Jiang, J. T. Zheng, Q. Liu and M. B. Wu, Degradation of azo dye using non-thermal plasma advanced oxidation process in a circulatory airtight reactor system, *Chem. Eng. J.*, 2012, **204–206**, 32–39.
28 J. Y. Chen, Y. L. Du, Z. J. Shen, S. S. Lu, K. Z. Su, S. J. Yuan, Z. H. Hu, A. Y. Zhang and J. W. Feng, Non-thermal plasma and $BiPO_4$ induced degradation of aqueous crystal violet, *Sep. Purif. Technol.*, 2017, **179**, 135–144.
29 V. Nair, A. Panigrahy and R. Vinu, Development of novel chitosan–lignin composite for adsorption of dyes and metal ions from wastewater, *Chem. Eng. J.*, 2014, **254**, 491–502.
30 S. X. Yang, L. Y. Wang, X. D. Zhang, W. J. Yang and G. L. Song, Enhanced adsorption of Congo red dye by functionalized carbon nanotube/mixed metal oxides nanocomposite derived from layer doubled hydroxide precursor, *Chem. Eng. J.*, 2015, **275**, 315–321.
31 V. O. Njoku, K. Y. Foo, M. Asif and B. H. Hameed, Preparation of activated carbons from rambutan (Nepheliumlappaceum) peel by microwave-induced KOH activation for acid yellow 17 dye adsorption, *Chem. Eng. J.*, 2014, **250**, 198–204.
32 X. X. Liu, W. P. Gong, J. Luo, C. T. Zou, Y. Yang and S. J. Yang, Selective adsorption of cationic dyes from aqueous solution by polyoxometalate-based metal-organic framework composite, *Appl. Surf. Sci.*, 2016, **362**, 517–524.
33 S. Faradi, M. M. Amini, M. Dusek, M. Kucerakova and F. Mahmoudi, A new nanohybrid material constructed

from Keggin-type polyoxometalate and Cd(II) semicarbazone Schiff base complex with excellent adsorption properties for the removal of cationic dye pollutants, *J. Mol. Struct.*, 2017, **1130**, 592–602.

34 Z. G. Jia, Z. Y. Li, T. Ni and S. B. Li, Adsorption of low-cost absorption materials based on biomass (Cortaderiaselloana flower spikes) for dye removal: Kinetics, isotherms and thermodynamic studies, *J. Mol. Liq.*, 2017, **229**, 285–292.

35 A. Bhattacharyya, D. Mondal, I. Roy, G. Sarkar, N. R. Saha, D. Rana, T. K. Ghosh, D. Mandal, M. Chakraborty and D. Chattopadhyay, Studies of the kinetics and mechanism of the removal process of proflavine dye through adsorption by grapheme oxide, *J. Mol. Liq.*, 2017, **230**, 696–704.

36 A. Regti, M. R. Laamari, S. E. Stiriba and M. E. Haddad, Use of response factorial design for process optimization of basic dye adsorption onto activated carbon derived from Persea species, *Microchem. J.*, 2017, **130**, 129–135.

37 D. H. Carrales-Alvarado, R. Ocampo-Perez, R. Leyva-Ramos and J. Rivera-Utrilla, Removal of the antibiotic metronidazole by adsorption on various carbon materials from aqueous phase, *J. Colloid Interface Sci.*, 2014, **436**, 276–285.

38 H. Li, N. H. An, G. Liu, J. L. Li, N. Liu, M. J. Jia, W. X. Zhang and X. L. Yuan, Adsorption behaviors of methyl orange dye on nitrogen-doped mesoporous carbon materials, *J. Colloid Interface Sci.*, 2015, **455**, 343–351.

39 L. Y. Zhang, H. Y. Zhang, W. Guo and Y. L. Tian, Removal of malachite green and crystal violet cationic dyes from aqueous solution using activated sintering process red mud, *Appl. Clay Sci.*, 2014, **93–94**, 85–93.

40 G. K. Sarma, S. S. Gupta and K. G. Bhattacharyya, Adsorption of Crystal violet on raw and acid-treated montmorillonite, K10, in aqueous suspension, *J. Environ. Manage.*, 2016, **171**, 1–10.

41 V. K. Gupta, S. Agarwal, A. Olgun, H. Demir, M. L. Yola and N. Atar, Adsorptive properties of molasses modified boron enrichment waste based nanoclay for removal of basic dyes, *J. Ind. Eng. Chem.*, 2016, **34**, 244–249.

42 R. L. Zhu, Q. Z. Chen, H. Y. Liu, F. Ge, L. F. Zhu, J. X. Zhu and H. P. He, Montmorillonite as a multifunctional adsorbent can simultaneously remove crystal violet, cetyltrimethylammonium, and 2-naphthol from water, *Appl. Clay Sci.*, 2014, **88–89**, 33–38.

43 Z. G. Jia, Z. Y. Li, T. Ni and S. B. Li, Adsorption of low-cost absorption materials based on biomass (Cortaderiaselloana flower spikes) for dye removal: Kinetics, isotherms and thermodynamic studies, *J. Mol. Liq.*, 2017, **229**, 285–292.

44 S. Shoukat, H. N. Bhatti, M. Iqbal and S. Noreen, Mango stone biocomposite preparation and application for crystal violet adsorption: A mechanistic study, *Microporous Mesoporous Mater.*, 2017, **239**, 180–189.

45 P. F. Sun, C. Hui, S. Wang, L. Wan and Y. H. Zhao, Bacillus amyloliquefaciens biofilm as a novel biosorbent for the removal of crystal violet from solution, *Colloids Surf., B*, 2016, **139**, 164–170.

46 S. S. Lam, R. K. Liew, Y. M. Wong, P. N. Y. Yek, N. L. Ma, C. L. Lee and H. A. Chase, Microwave-assisted pyrolysis with chemical activation, an innovative method to convert orange peel into activated carbon with improved properties as dye adsorbent, *J. Cleaner Prod.*, 2017, **162**, 1376–1387.

47 E. Lakovleva, M. Sillanpaä, P. Maydannik, J. T. Liu, S. Allen, A. B. Albadarin and C. Mangwandi, Manufacturing of novel low-cost adsorbent: Co-granulation of limestone and coffee waste, *J. Environ. Manage.*, 2017, **203**, 853–860.

48 R. P. Chicinaş, H. Bedelean, R. Stefan and A. Măicăneanu, Ability of a montmorillonitic clay to interact with cationic and anionic dyes in aqueous solutions, *J. Mol. Struct.*, 2018, **1154**, 187–195.

49 P. S. Thue, A. C. Sophia, E. C. Lima, A. G. N. Wamba, W. S. de Alencar, G. S. dos Reis and F. S. Rodembusch, Synthesis and characterization of a novel organic-inorganic hybrid clay adsorbent for the removal of acid red 1 and acid green 25 from aqueous solutions, *J. Cleaner Prod.*, 2018, **171**, 30–44.

50 Y. Zheng, D. Y. Chen, N. J. Li, Q. F. Xu, H. Li, J. H. He and J. M. Lu, Highly efficient simultaneous adsorption and biodegradation of a highly-concentrated anionic dye by a high-surface-area carbon-based biocomposite, *Chemosphere*, 2017, **179**, 139–147.

51 N. Tahir, H. N. Bhatti, M. Lqbal and S. Noreen, Biopolymers composites with peanut hull waste biomass and application for Crystal Violet adsorption, *Int. J. Biol. Macromol.*, 2017, **94**, 210–220.

52 S. Shoukat, H. N. Bhatti, M. Lqbal and S. Noreen, Mango stone biocomposite preparation and application for crystal violet adsorption: A mechanistic study, *Microporous Mesoporous Mater.*, 2017, **239**, 180–189.

53 N. Tahir, H. N. Bhatti, M. Iqbal and S. Noreen, Biopolymers composites with peanut hull waste biomass and application for Crystal Violet adsorption, *Int. J. Biol. Macromol.*, 2017, **94**, 210–220.

54 X. G. Cai, J. Y. He, L. Chen, Y. L. Li, K. S. Zhang, Z. Jin, J. Y. Liu, C. M. Wang, X. G. Wang and L. T. Kong, A 2D-g-C_3N_4 nanosheet as an eco-friendly adsorbent for various environmental pollutants in water, *Chemosphere*, 2017, **17**, 192–201.

55 X. R. Ding, J. Zhu, Y. Zhang, Q. Xia, W. T. Bi, X. D. Yang and J. F. Yang, Separation and concentration of natural products by fast forced adsorption using well-dispersed velvet-like graphitic carbon nitride with response surface methodology optimization, *Talanta*, 2016, **154**, 119–126.

56 N. Bao, X. D. Hu, Q. Z. Zhang, X. H. Miao, X. Y. Jie and S. Zhou, Synthesis of porous carbon-doped g-C_3N_4 nanosheets with enhanced visible-light photocatalytic activity, *Appl. Surf. Sci.*, 2017, **403**, 682–690.

57 G. Mamba and A. K. Mishra, Graphitic carbon nitride (g-C_3N_4) nanocomposites: A new and exciting generation of visible light driven photocatalysts for environmental pollution remediation, *Appl. Catal., B*, 2016, **198**, 347–377.

58 S. W. Cao, J. X. Low, J. G. Yu and M. Jaroniec, Polymeric photocatalysts based on graphitic carbon nitride, *Adv. Mater.*, 2015, **27**, 2150–2176.

59 G. Q. Tan, L. N. She, T. Liu, C. Xu, H. J. Ren and A. Xia, Ultrasonic chemical synthesis of hybrid mpg-C_3N_4/$BiPO_4$

heterostructured photocatalysts with improved visible light photocatalytic activity, *Appl. Catal., B*, 2017, **207**, 120–133.

60 C. Y. Liu, Y. H. Zhang, F. Dong, A. H. Reshak, L. Q. Ye, N. Pinna, C. Zeng, T. R. Zhang and H. W. Huang, Chlorine intercalation in graphitic carbon nitride for efficient photocatalysis, *Appl. Catal., B*, 2017, **203**, 465–474.

61 X. B. He, F. X. Yin, J. N. Chen and C. Y. Ye, Co-$SrCO_3$/N-doped carbon: a highly efficient hybrid electrocatalyst for the oxygen reduction reaction and Zn–air batteries, *Inorg. Chem. Front.*, 2017, **4**, 1073–1086.

62 W. C. Zhu, G. L. Zhang, J. Li, Q. Zhang, X. L. Piao and S. L. Zhu, Hierarchical mesoporous $SrCO_3$ submicron spheres derived from reaction-limited aggregation induced "rod-to-dumbbell-to-sphere" self-assembly, *CrystEngComm*, 2010, **12**, 1795–1802.

63 J. M. Du, Z. M. Liu, Z. H. Li, B. X. Han, Y. Huang and J. L. Zhang, Synthesis of mesoporous $SrCO_3$ spheres and hollow $CaCO_3$ spheres in room-temperature ionic liquid, *Microporous Mesoporous Mater.*, 2005, **83**, 145–149.

64 W. C. Zhu, Z. Z. Liang, X. F. Liu, H. Zhang, Y. J. Zheng, X. L. Piao and Q. Zhang, Soft-template self-assembly of hierarchical mesoporous $SrCO_3$ by low-temperature hydrothermal route and their application as adsorbents for methylene blue and heavy metal ions, *Powder Technol.*, 2012, **226**, 165–172.

65 S. S. Wu, S. F. Yin, H. Q. Cao, Y. X. Lu, J. F. Yin and B. J. Li, Glucosan controlled biomineralization of $SrCO_3$ complex nanostructures with superhydrophobicity and adsorption properties, *J. Mater. Chem.*, 2011, **21**, 8734–8741.

66 X. Bai, L. Wang, R. Zong and Y. Zhu, Photocatalytic activity enhanced *via* g-C_3N_4 nanoplates to nanorods, *J. Phys. Chem.*, 2013, **117**, 9952–9961.

67 W. N. Xing, C. M. Li, G. Chen, Z. H. Han, Y. S. Zhou, Y. D. Hu and Q. Q. Meng, Incorporating a novel metal-free interlayer into g-C_3N_4 frame work for efficiency enhanced photocatalytic H_2 evolution activity, *Appl. Catal., B*, 2017, **203**, 65–71.

68 S. B. Ni, W. L. Yang and T. Li, Hydrothermal synthesis and photoluminescence properties of $SrCO_3$, *Mater. Lett.*, 2011, **65**, 766–768.

69 A. Tahmasian, V. Safarifard, A. Morsali and S. W. Joo, Sonochemical syntheses of a new fibrous-like nano-scale strontium(II) 3D coordination polymer; precursor for the fabrication of a strontium carbonate nanostructure, *Polyhedron*, 2014, **67**, 81–88.

70 Z. F. Huang, J. J. Song, L. Pan, Z. M. Wang, X. Q. Zhang, J. J. Zou, W. B. Mi, X. W. Zhang and L. Wang, Carbon nitride with simultaneous porous network and O-doping for efficient solar-energy-driven hydrogen evolution, *Nano Energy*, 2015, **12**, 646–659.

71 W. K. Jo and C. S. Selvam, Enhanced visible light-driven photocatalytic performance of ZnO-g-C_3N_4 coupled with graphene oxide as a novel ternary nanocomposite, *J. Hazard. Mater.*, 2015, **299**, 462–470.

72 D. M. Chen, J. J. Yang and H. Ding, Synthesis of nanoporous carbon nitride using calcium carbonate as templates with enhanced visible-light photocatalytic activity, *Appl. Surf. Sci.*, 2017, **391**, 384–391.

73 I. Papailias, T. Giannakopoulou, N. Todorova, D. Demotukali, T. Vaimakis and C. Trapalis, Effect of processing temperature on structure and photocatalytic properties of g-C_3N_4, *Appl. Surf. Sci.*, 2015, **358**, 278–286.

74 Y. X. Zhang, J. Wu, Y. Y. Deng, Y. J. Xin, H. L. Liu, D. Ma and N. Bo, Synthesis and visible-light photocatalytic property of Ag/GO/g-C_3N_4 ternary composite, *J. Mater. Sci. Eng. B*, 2017, **211**, 1–9.

75 M. Wu, J. M. Yan, X. N. Tang, M. Zhao and Q. Jiang, Synthesis of potassium-modified graphitic carbon nitride with high photocatalytic activity for hydrogen evolution, *ChemSusChem*, 2014, **7**, 2654–2658.

76 M. Wu, J. M. Yan, X. W. Zhang and M. Zhao, Synthesis of g-C_3N_4 with heating acetic acid treated melamine and its photocatalytic activity for hydrogen evolution, *Appl. Surf. Sci.*, 2015, **354**(44), 195–200.

77 J. L. Lv, K. Dai, J. F. Zhang, Q. Liu, C. H. Liang and G. P. Zhu, Facile constructing novel 2D porous g-C_3N_4/BiOBr hybrid with enhanced visible-light-driven photocatalytic activity, *Sep. Purif. Technol.*, 2017, **178**, 6–17.

78 S. Álvarez-Torrellas, R. S. Ribeiro, H. T. Gomes, G. Ovejero and J. García, Removal of antibiotic compounds by adsorption using glycerol-based carbon materials, *Chem. Eng. J.*, 2016, **295**, 277–288.

79 Y. S. Ho and G. McKay, Pseudo-second order model for sorption processes, *Process Biochem.*, 1999, **34**, 451–465.